Electrochemical Plasmonic Optical Fiber Probe for Real-time Insight into Coreactant Electrochemiluminescence

Jingxian Yu,[a,*] Peipei Jia,[a] Shengping Wang,[b] Heike Ebendorff-Heidepriem,[a] and Andrew D. Abell[a]

[a] ARC Centre of Excellence for Nanoscale BioPhotonics (CNBP), Institute of Photonics and Advanced Sensing (IPAS), School of Physical Sciences, The University of Adelaide, SA 5005, Australia

[b] Faculty of Materials Science and Chemistry, China University of Geosciences, Wuhan 430074, China

* Corresponding author
E-mail address: jingxian.yu@adelaide.edu.au.

Abstract

Electrochemical surface plasmon resonance (ESPR) is a powerful technique for defining dynamic changes in chemical composition and morphology of functional interfaces by correlating spectral information with voltammetric characteristics of the electrode processes. However, conventional Kretschmann prism-based surface plasmon resonance (SPR) configurations require sophisticated apparatus and complex optics. Here, we present a versatile flow injection ESPR device that incorporates a plasmonic and conductive fiber optic probe, for which a gold nanohole array film is integrated onto the endface of a conventional optical fiber via template transfer. The coreactant-based $Ru(bpy)_3^{2+}$ / tripropylamine (TPrA) electrochemiluminescence (ECL) system, was chosen to unravel electrochemically-induced real-time interfacial information, since such an approach is increasingly employed for clinical assay analysis and the associated ECL mechanism is an active area of investigation. The ESPR observations provide novel experimental evidence to support the proposition that the ECL reactions undergo an oxidative-reduction pathway. Moreover, the ESPR peak shift exhibits a broader linear detection range of TPrA concentration (0.02 - 20 mmol L^{-1}, R^2=0.996), compared to the ECL and SPR techniques (< 10 mmol L^{-1}). This study clearly demonstrates that the novel fiber optic ESPR device presents as a reliable and multimodal spectroelectrochemical platform to gain mechanistic insights into complicated chemical processes and provide sensing capabilities, while offering great simplicity, portability and miniaturization.

Keywords: Electrochemical Surface Plasmon Resonance; Gold Nanohole Array Film; Plasmonic Fiber Optic Probe; Electrochemiluminescence.

1. Introduction

Electrochemical surface plasmon resonance (ESPR) allows chemical reactions to be electrically manipulated on the interface of the electrode, while simultaneously collecting the corresponding optical response (i.e. the changes in local refractive index)[1] and voltammetric characteristics of the electrode reaction processes.[2, 3] This offers a promising means to examine and monitor interactions between small molecules, for example potential drugs and biological films (e.g. biomolecules, cancer cells, or bacterial),[4-7] an understanding of which is vital for developing biosensors[8] and bioenergy harvesting devices.[9] The majority of such ESPR measurements are carried out using commercial surface plasmon resonance (SPR) equipment based on the Kretschmann configuration,[10-13] a prism-based approach that is bulky and necessitating the use of complex optics and apparatus. This also prohibits remote sensing and online monitoring applications.[14] In this regard, fiber optic based ESPR devices present as a compact and efficient strategy to circumvent these limitations, and provides ease of integration with disposable and portable sensing chips.[15-17] A good deal of recent effort has gone into integrating electrochemistry and grating-assisted SPR within a single miniaturized optical fiber.[18, 19] In particular, Guo and Zhou[20] reported a novel ESPR sensor for monitoring electroactive biofilms in situ using a commercial single-mode fiber coated with a nanoscale gold film, which generated SPR signals while also serving as the working electrode. A tilted fiber Bragg grating (TFBG) was written into the fiber to enhance SPR excitations. Smietana[21] investigated the electrode processes of an electrochemical redox pair using a long-period fiber grating functionalized by conductive indium tin oxide (ITO), where the ITO film promoted the sensitivity of the fiber grating to the change of local refractive index.

Notably, ultrathin metal films with periodic nanohole arrays[22] known to produce plasmonic signals with significantly improved sensitivity[23, 24] have gained extensive attention for their biological and environmental sensing applications.[25, 26] In this context, we have recently reported the optical fiber-based nanoplasmonic probe for biological sensing,[27, 28] where the endface of a conventional optical fiber is functionalized with a gold nanohole array film via the template transfer technique. This allows collection of plasmonic response in a transmission mode at normal incidence that differs from the prism-based SPR system,[15, 29] to simplify optical system design, and also offers great portability, low cost and miniaturization. Further to this, the fiber-based probe presents as an elegant integration of spectroscopic functionality (i.e. SPR) and electrical conduction (i.e. metal electrode),[30-34] thus offers an unprecedented opportunity to explore electrically modulated SPR responses and their potential use in sensing. With this in mind, we now move one step further to fabricate a flow injection ESPR device by incorporating the plasmonic fiber probe together with other electrochemical components (i.e. reference and counter electrodes) into the flowing channel, where the plasmonic probe also acts as the working electrode. This novel ESPR device allows to concurrently gather the optical and voltametric responses occurring on the probe, while the electrode potential of the probe is electrochemically manipulated. As SPR is highly sensitive to the dielectric properties on the electrolyte/probe interface, electrochemically modulated oxidation/reduction reactions and the consequent diffusion layers can be monitored by SPR. This offers an abiliity to quantitatively measure the real-time changes in local physical properties (e.g. refractive index) associated with the electrochemical reactions, with an opportunity to provide novel sensing tools and resolve complicated reaction mecanisms. It is worth mentioning that this device is multimodal and versatile, that can work as an independent electrochemical or optical sensor if necessary, while being an integrated electrochemical-optical platform even beyond ESPR.

The coreactant-based $Ru(bpy)_3^{2+}$ / tripropylamine (TPrA) electrochemiluminescence (ECL) model system was therefore chosen for this study to unravel electrochemically-induced real-time interfacial information, since this ECL system is increasingly employed for clinical assay analysis.[35-37] However, the underlying ECL mechanism is an active area of investigation,[38, 39] with numerical simulations commonly employed to verify the mechanistic hypotheses[40, 41] and lacking real-time interfacial information. The newly developed flow injection electrochemical device will be first employed to produce ECL results that are then compared to the reported data in literature, to validate the electrochemical-optical performance. Next, the real-time multi-dimensional interfacial ESPR information will be acquired to gain mechanistic insights into the complicated chemical and electrochemical ECL processes. Finally, all the ECL, SPR and ESPR signals collected through the two steps above will be cross-checked to verify the multimodal sensing ability of the fiber-based sensor. With respect to the prism-based ESPR system, this study demonstrates the electrochemical fiber-based plasmonic probe is a versatile and multimodal platform to produce real-time multi-dimensional interfacial information with an ability to tackle fundamental questions and practical sensing applications, while also offering great simplicity, portability, low cost and miniaturization. Moreover, this novel device provides an opportunity to advance the development of multiplexed imaging by electrochemical potential sweep and spatial translation of the fiber optic probe in the future.

2. Materials and methods

2.1. Fabrication of the nanoplasmonic fiber optic probe

A schematic of the fabrication of the gold nanohole array on the end-face of an optical fiber by template transfer is illustrated in Figure 1a. A periodic hexagonal pattern of nanoholes (Figure 1a, Si template) carved in a silicon wafer, was chosen as a template for gold film deposition, since the associated hexagonal hole array can greatly suppress resonance crosstalk

in comparison to other nanohole arrangement patterns, for example a square hole array.[28, 42] A gold layer of 100 nm thickness was deposited onto the Si template (Figure 1a, gold deposition) by a thermal evaporator (Emitech K975x MVD, Quorum Tech, UK), in order to translate the hexagonal pattern into the resulting nanohole array film. Next, the patterned gold film was transferred to the polished fiber end-face through a thin epoxy adhesive layer (Figure 1a, template transfer). Following epoxy curing, the Si template was gently removed to give a nanohole array gold film on the tip of an optical fiber (Figures 1a and 1b).

An SEM image of this film reveals that the gold film presents a hexagonal array arrangement of homogenous nanoholes (see Figure 1c), with a nearest hole-hole distance of 700 nm and a hole diameter of 200 nm. The nanohole array film typically has a diameter of several millimeters and covers the entire fiber end-face to eliminate edge effects of light scattering at the fiber optic core. Localized SPR responses on such patterned gold films were fully characterized in support of digital simulations in our earlier study.[28] The corresponding primitive unit cell is illustrated by the green dashed rhombus (Figure 1c, inset), to give a porosity of 7.5% for the nanohole array film. Notably, this fabrication process allows for the Si template to be re-used after chemical cleaning, and hence reduces the expensive and time-consuming regeneration of Si templates. This highlights the reproducibility and robust nature of the template transfer technique. The electrical contact between the periodic nanohole array gold film and the metallic fiber ferrule was made in the final step by conductive carbon glue. The resultant fiber plasmonic probe combines both spectroscopic functionality (i.e. plasmonic resonance) and electric conduction onto the same tip of the fiber to provide a new avenue for the design and development of miniaturized spectroscopic-electrochemical devices.

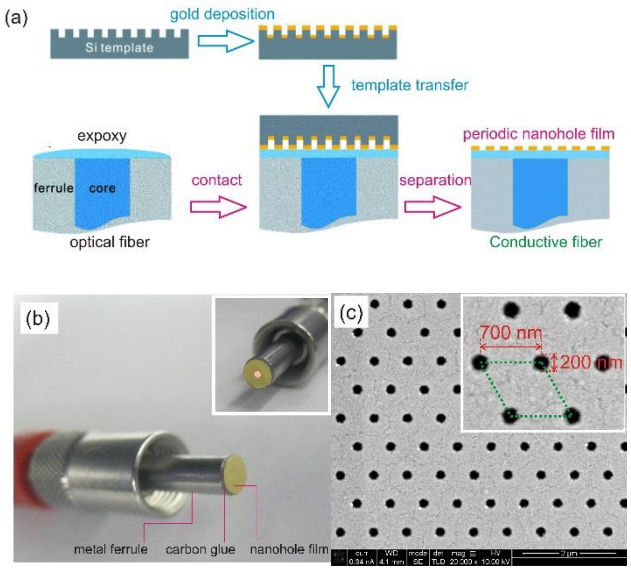

Figure 1. (a) Fabrication of periodic nanohole gold film on the endface of an optical fiber by template transfer. (b) Photograph of optical fiber tip after a gold nanohole film transferred. Inset: Illuminated by coupling white light from the distant end. (c) SEM image of the hexagonal nanohole array film and corresponding primitive unit cell (green dashed rhombus).

2.2. Assembly of flow injection fiber optic ESPR device.

The fiber nanoplasmonic probe was incorporated into a flow cell made by polydimethylsiloxane (PDMS, Sigma-Aldrich, Australia), with the gold nanohole array film exposed to the fluidic channel and aligned parallel to the flow direction (see Figure 2). The nanohole film formed the working electrode (WE) by wire connection to an Autolab PGSTAT204 electrochemical analyzer (Metrohm Autolab, the Netherlands). The other end of the plasmonic fiber was coupled to a tungsten halogen white light source (HL-2000, Ocean Optics Inc, USA), allowing the fiber core to guide incident light to the gold nanohole film. Light passing through the nanohole array film, from an external light source, was collected by the other face-to-face configured fiber, to deliver the transmission signal to a spectrometer (USB4000, Ocean Optics Inc, USA). All transmission spectra were reported with reference to the light source in the wavelength range between 350 nm and 1050 nm. Electrochemically generated chemiluminescence on the probe is collected, when the external light source switched off.

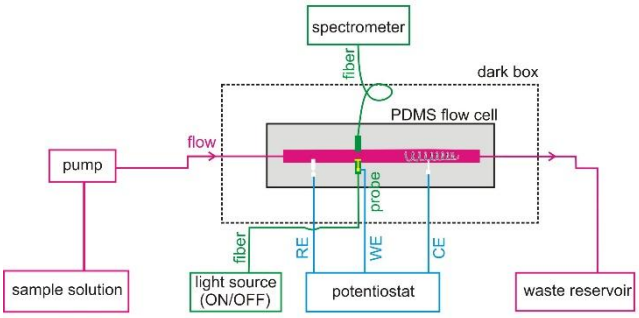

Figure 2. Assembly schematic of flow injection fiber optic ESPR device.

2.3. Electrochemical measurements.

Phosphate buffer solution (PBS, 0.1 mol L^{-1}, pH = 7.4) containing 1.0 mmol L^{-1} tris(bipyridine) ruthenium(II) chloride (99.95%, Sigma-Aldrich, Australia) and a varied concentration of tripropylamine (TPrA 98%, Sigma-Aldrich, ranging from 0-20 mmol L^{-1}) was injected from the inlet (see Figure 2). The flow was subsequently passed through the channel over the reference electrode (RE, AgCl/Ag wire), followed by the fiber optic plasmonic probe (i.e. working electrode), and finally the counter electrode (CE, coiled platinum wire). Fluid motion was maintained at a flow rate of 0.050 mL min^{-1} by a programmable PHD 2000 syringe pump (Harvard Apparatus, USA). The flow injection device was first tested with water to ensure that a reproducible and previously reported transmission spectrum[43] was observed. All measurements were conducted at 25 ^{o}C.

3. Results and discussion

3.1. Electrochemiluminescence.

A well-described coreactant $Ru(bpy)_3^{2+}$ / TPrA ECL system was chosen to evaluate the electrochemistry and spectroscopy performance of the fabricated ESPR device, since it exhibits high luminescence efficiency while providing great simplicity in experimental design. With the external light source switched off (see Figure 2), cyclic voltammograms and the corresponding ECL emission spectra were recorded in 1.0 mmol L^{-1} $Ru(bpy)_3Cl_2$ and 0.1 mol

L^{-1} phosphate buffer solution (pH = 7.4), in the absence and presence of tripropylamine (TPrA). The potential sweeps commenced at 0.0 V (vs AgCl/Ag), ramping up to a vertex potential of 1.3 V and then returning back to 0.0 V at a scan rate of 50 mV s^{-1}. Simultaneously, 520 of ECL emission spectra (350 nm - 1050 nm) were captured per voltammetric cycle with a contant time interval through the face-to-face coupled fiber spectrometer (see Figure 2). In the absence of TPrA, the cyclic voltammogram of $Ru(bpy)_3^{2+}$ exhibits a pair of redox peaks between 0.85 and 0.95 V (Figure 3a, blue curve), indicating a one-electron oxidation/reduction reaction of $Ru(bpy)_3^{2+}$. Similar observations have been reported on a flat gold electrode,[44-46] demonstrating that the fiber optic probe shares similar electrochemical characteristics to a conventional gold electrode. This clearly indicates that electrical conduction (i.e. the nanohole array gold film) is successfully integrated into the electrical loop, being a novel functionality to the conventional optical fiber. The ECL spectrum captured at 1.1 V (Figure 3b, blue curve) shows the appearance of a maximum at 614 nm, indicative of the emission of excited $Ru(bpy)_3^{2+}$ state.[45, 47] It is known that this emission correspondes to an ion annihilation process of the excited $Ru(bpy)_3^{2+}$ state.[48, 49] The corresponding potential-dependent ECL peak intensity is weak over the entire voltammetric cycle (Figure 3c, blue curve).

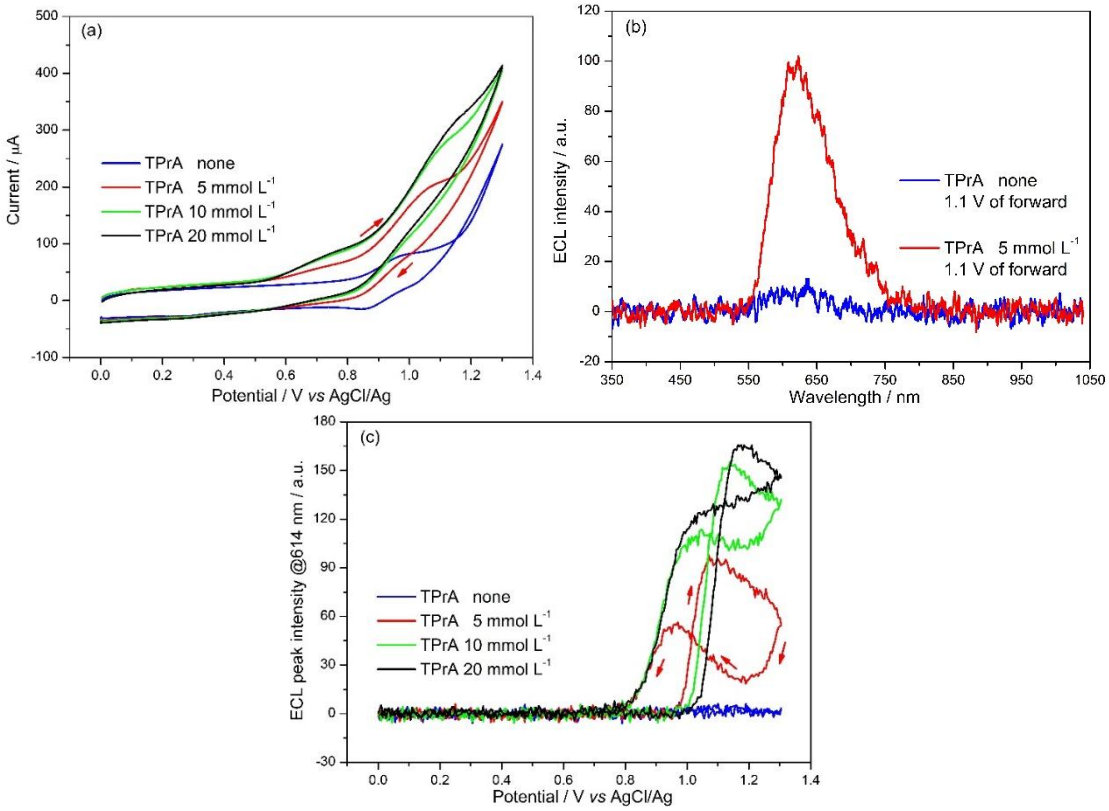

Figure 3. (a) Cyclic voltammograms on the fiber optic probe in 1.0 mmol L^{-1} $Ru(bpy)_3Cl_2$ and 0.1 mol L^{-1} PBS (pH = 7.4) solutions containing a varied concentration of TPrA at a scan rate of 50 mV s^{-1}. (b) ECL spectra collected at 1.1 V in the absence and presence of TPrA. (c) Potential-dependent ECL peak intensities at 614 nm.

In contrast, the ECL emission at 1.1 V (Figure 3b, red curve) is remarkably intensified in the presence of 5.0 mmol L^{-1} TPrA. In particular, the potential-dependent ECL peak intensity begins to increase at 0.95 V and rapidly reaches a maximum around 1.1 V (see Figure 3c, red curve). On the reverse scan, the ECL signal continues to decrease with a minimum appearing at 1.2 V. Accordingly, an increase in the oxidation current appears at 0.6 V (see Figure 3a, red curve), different to the value of 0.95 V observed in the absence of TPrA (Figure 3a, blue curve). It is believed that the increase in current is attributable to the electrochemical oxidation of TPrA.[44, 45] The electrochemical current above 0.95 V features the coreactant oxidation of $Ru(bpy)_3^{2+}$, as evidenced by the enhanced ECL emission (Figure 3b, red curve). In the presence of higher TPrA concentrations (i.e. 10 and 20 mmol L^{-1}), both ECL emission intensity and electrochemical oxidation current further increase, but with a reduced gradient (see Figure 3, green and black curves). This underscores the qualitative and quantitative

features of the electrochemical fiber optic device. Further mechanistic insights into this ECL system will be provided through the in-situ multi-dimensional ESPR results as discussed below.

3.2. Electrochemical Surface Plasmon Resonance.

With the electrochemical-optical performance of the fiber optic device demonstrated, we next set out to investigate the ESPR responses. The external light source was switched on (see Figure 2), and the resulting potential-dependent transmission spectra (i.e. 520 sets per voltammetric cycle) were recorded in the same solutions. In the absence of TPrA, the transmission spectrum captured at 0.0 V vs AgCl/Ag displays multiple peaks and troughs (Figure 4a, blue curve). In particular, the peaks (eg. peak1 at 830.2 nm and peak2 at 899.0 nm) and dip (eg. dip1 at 853.3 nm) have narrow full-widths at half-maxima (FWHM), a typical value of 25 nm, which is similar to the SPR line width reported earlier on this probe where no electrochemistry was coupled.[27, 28] Increasing the electrode potential from 0.0 V to 1.1 V, shifts these peaks to longer wavelengths, namely 832.1 nm, 855.1 nm, and 901.2 nm (see Figure 4a, red curve) respectively, whilst the intensity of these peaks decreases. In contrast, other peaks (or dips) almost remain unchanged. The peak at 500 nm (see Figure 4a, blue curve) is attributed to the intrinsic electron transitions and coactions between the conduction band and the d-energy band of gold, while the peak at 950 nm is responsible for the SPR resonance on the fiber side of the gold film.[28] They do not directly interact with the electrolyte. It is worth noting that the ECL reactions also take place at 1.1 V, with an emission peak appearing at 614 nm (see Figure 3). Interestingly, the transmission intensity around this wavelength (for example between 575 nm and 675 nm, red curve in Figure 4a) is slightly lower than that at 0.0 V (blue curve in Figure 4a). The decrease in SPR transmission intensity (approx. 10%) is likely induced by the ECL emission,[46, 50] and consistent with our previously reported localized SPR excitation on these patterned films.[28] This ECL induced

SPR excitation helps to explain the relatively weak ECL intensities observed in Section 3.1. All SPR peaks (and dip) share a very similar potential-dependent manner. The wavelength of peak2, the furthest from the ECL emission wavelength, is thus chosen and depicted over the electrode potential (see Figure 4b, blue curve). The SPR peak begins to appear at 899.04 nm and remains unchanged until 0.3 V, then gradually red-shifts up to the vertex of 1.3 V. On the reverse scan, the SPR peak continues shifting to longer wavelengths from 1.3 to 1.1 V, then slowly decreases beyond this potential. However, it does not return to the initial value at 0 V, remaining ~ 1 nm longer. Similar observations have been reported previously,[39, 51] and are likely due to the hysterisis of mass transport induced by electrochemical reactions at the vicinity of the probe. Both λ_{max} and λ_{min} are defined as the global maximum and mininum of SPR peak wavelengths over the cyclic sweep between 0.0 V and 1.3 V (vs AgCl/Ag). The λ_{max} and λ_{min} values are found to be 901.01 nm and 899.04 nm (Figure 4b, blue curve), giving a shift (i.e. λ_{max} - λ_{min}) of 1.97 nm.

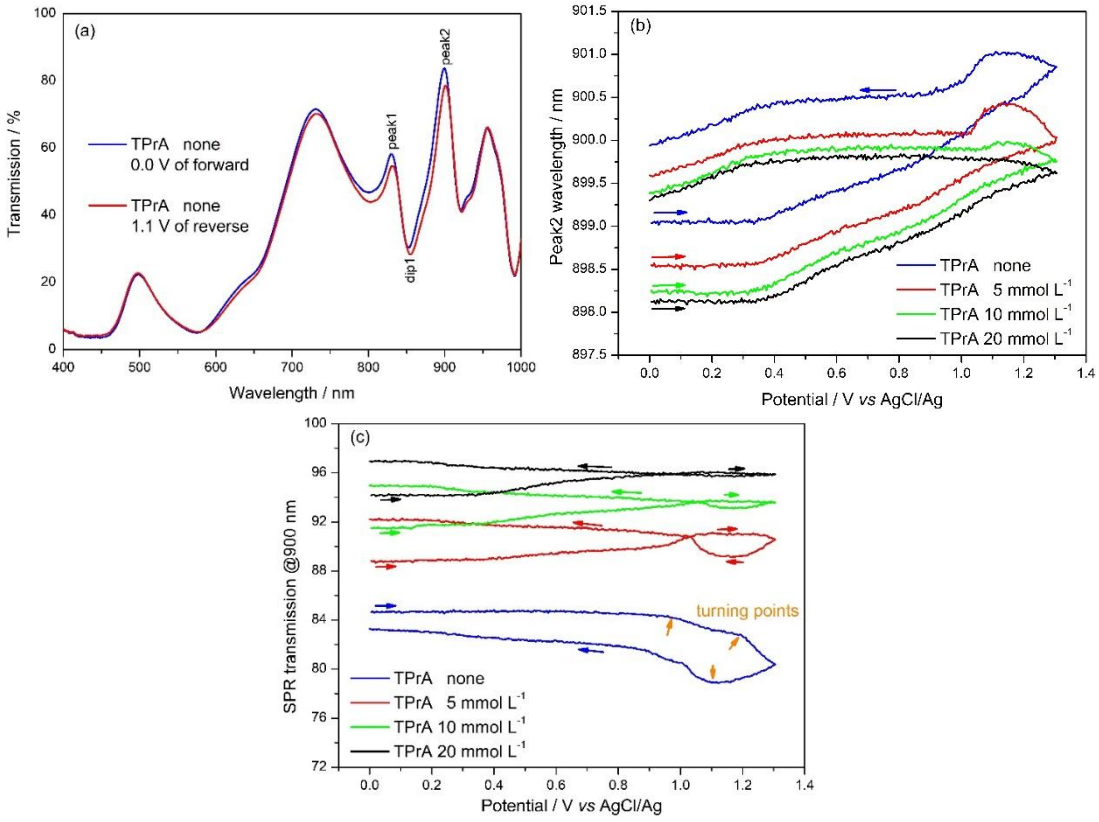

Figure 4. (a) Transmission spectra through the fiber optic probe at different potentials during a cyclic voltammetric measurement in 1.0 mmol L^{-1} $Ru(bpy)_3Cl_2$ and 0.1 mol L^{-1} PBS (pH = 7.4) solution. (b) Potential-

dependent SPR peak wavelengths and (c) SPR transmission intensities at 900 nm in 1.0 mmol L^{-1} $Ru(bpy)_3Cl_2$ and 0.1 mol L^{-1} PBS (pH = 7.4) solutions containing a varied concentration of TPrA at a scan rate of 50 mV s^{-1}.

In the presence of 5.0 mmol L^{-1} TPrA, the cyclic ESPR curve (Figure 4b, red curve) is similar to the shape of the aforementioned curve (blue curve), but with a blue-shift of ~ 0.7 nm. This reflects the dielectric changes on the probe/solution interface, due to addition of TPrA. The SPR peak begins to appear at a minimum of 898.51 nm, and attains a maximum λ_{max} at 1.1 V on the reverse scan, giving a slightly smaller shift (λ_{max} - λ_{min}) of 1.88 nm. With a further increase in TPrA concentration (i.e. 10 and 20 mmol L^{-1}), the ESPR curves shift to even shorter wavelengths, however a reducing blue-shift is apparent. The λ_{min} values appear at 898.21 nm and 898.12 nm respectively for 10 and 20 mmol L^{-1} of TPrA, giving (λ_{max} - λ_{min}) shifts of 1.77 nm and 1.63 nm. Clearly, the ESPR peak shift (λ_{max} - λ_{min}) is sensitive to TPrA concentration. Notably, the ESPR peak at 1.1 V reduces and eventually disappears at 20 mmol L^{-1} of TPrA (Figure 4b, black curve). This reflects electrochemically-induced dielectric changes on the probe/solution interface, [32, 33] including reconstructions of electrochemical double layers and reactants / products diffusion layers.

The SPR transmission intensity at 900 nm (near the SPR peak) is also depicted over the electrode potential in Figure 4c to visualize the electrode process occurring on the probe/solution interface. In the absence of TPrA, the SPR transmission remains essentially unchanged (Figure 4c, blue curve) up to 0.95 V vs AgCl/Ag. Electrochemical oxidation $Ru(bpy)_3^{2+} \rightarrow Ru(bpy)_3^{3+}$ takes place at this potential, as indicated by the increase in current (Figure 3a, blue curve). The surface concentration of $Ru(bpy)_3^{3+}$ begins to accumulate and is controlled by a limiting diffusion process of $Ru(bpy)_3^{2+}$ up to 1.2 V, as indicated by the CV curves (see Figure 3a). As a result, the SPR transmission intensity continues to decrease (see Figure 4c, blue curve). Notably, a slightly more rapid transmission decrease is observed beyond 1.2 V, which corresponds to the steep rise of oxidation current (see Figure 3a, blue

curve). This is likely attributable to the evolution of O_2.[45] The accumulation of $Ru(bpy)_3^{3+}$ continues until 1.1 V on the reverse scan, where the corresponding SPR transmission curve reaches a minimum. The electrochemical current becomes negative at lower potentials (see Figure 3a, blue curve), indicating occurence of the reduction reaction $Ru(bpy)_3^{3+} \rightarrow Ru(bpy)_3^{2+}$. The surface concentration of $Ru(bpy)_3^{2+}$ begins to restore, as confirmed by the rebounding transmission intensity observed (see Figure 4c, blue curve).

In the presence of 5.0 mmol L^{-1} TPrA, the SPR transmission at 900 nm (see Figure 4c, red curve) gradually increases beyond 0.6 V vs AgCl/Ag, due to electrochemical oxidation of TPrA (Figure 3a, red curve). The transmission quickly takes an ‘S‘ turn at 1.0 V to be a flat line, where the electrochemical oxidation of $Ru(bpy)_3^{2+}$ begins to take place as evidenced by the voltammogram and ECL emission (see Figure 3). SPR transmission intensity then slowly declines down to 1.1 V on the reverse scan, and takes another ‘S‘ turn at 1.0 V to a climbing line back to 0.0 V. A distinctive SPR transmission intensity loop spans between 1.0 V and 1.3 V (Figure 4c, red curve), in consistent with the ECL emission loop (Figure 3c, red curve. This contrasts to the observation in the absence of TPrA (Figure 4c, blue curve), suggesting a different ECL reaction mechanism. Several competitive reaction pathways have been proposed for this ECL system,[37, 52] for example an oxidative-reduction pathway[41] and the TPrA oxidation-driven pathway.[53] We believe that the oxidative-reduction pathway illustrated in Figure 5, better describes the observations here.

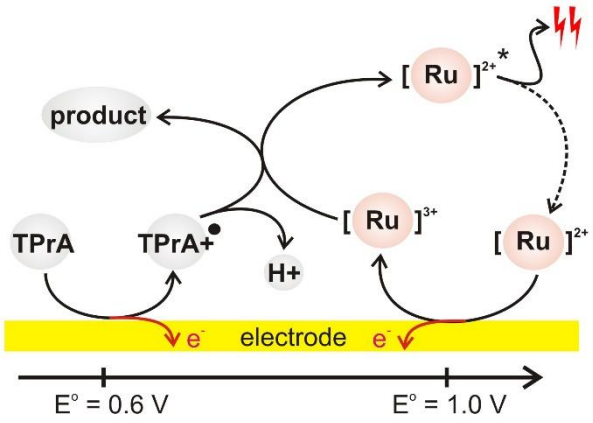

Figure 5. Oxidative-reduction pathway for the coreactant $Ru(bpy)_3^{2+}$ / TPrA ECL system.

Direct oxidation of TPrA takes place at 0.6 V vs AgCl/Ag as indicated by the SPR transmission curve (Figure 4c, red curve), leading to accumulation of TPrA+ radicals and also consumption of TPrA (see Figure 5). The oxidation $Ru(bpy)_3^{2+} \rightarrow Ru(bpy)_3^{3+}$ begins to take place at 1.0 V, and the $Ru(bpy)_3^{3+}$ generated instantaneously reacts with the accumulated TPrA+ radicals to yield the excited state of $Ru(bpy)_3^{2+}*$ through a homogenous reaction. The excited state quickly releases ECL emission to regenerate $Ru(bpy)_3^{2+}$ on the interface. Although the generation of TPrA+ radicals is a limiting diffusion process when the potential shifting to a more positive value (for example 1.2 V), the regeneration ensures a relatively stable level of $Ru(bpy)_3^{2+}$. The flat SPR transmission intensity observed between 1.0-1.2 V (Figure 4c, red curve), reflects a tentative equilibrium between the two intermediates, namely $Ru(bpy)_3^{3+}$ and TPrA+. Evolution of O_2 begins beyond 1.2 V, which quenches $Ru(bpy)_3^{2+}*$ as evidenced by the reduced ECL intensity (see Figure 3c, red curve). A further increase in the oxidation current of $Ru(bpy)_3^{2+}$ facilitates the accumulation of $Ru(bpy)_3^{3+}$. This corresponds to the slow decrease of transmission intensity from 1.2 V of the forward scan to 1.1 V of the reverse scan. The electrochemical oxidation of $Ru(bpy)_3^{2+}$ discontinues (see Figure 3a, red curve) at potentials lower than 1.0 V within the reverse scan, allowing TPrA+ radicals to build up at the interface.

Since the limiting diffusion of TPrA is proportional to its bulk concentration according to Fick's 1st law of diffusion,[54] a higher TPrA concentration (i.e. 10 and 20 mmol L^{-1}) produces a greater flux of TPrA+ radicals. In turn, a greater flux of TPrA+ radicals slows down the accumulation of $Ru(bpy)_3^{3+}$, also with more $Ru(bpy)_3^{2+}$ regenerated to yield the excited state of $Ru(bpy)_3^{2+}*$. Not surprisingly, a reducing SPR loop size is observed (see Figure 4c, green and black curves). Clearly, these results demonstrated that the novel flow injection ESPR sensor is multimodal and multi-dimensional platform to visualize electrochemically-induced dynamic interfacial changes, and provides real-time evidence to support the ECL mechanistic proposition.

3.3. Cross-checked detection of TPrA.

As discussed above, both the ECL peak intensity (see Figure 3c) and the SPR peak wavelength (λ_{min}) (see Figure 4b) are highly sensitive to the concentration of TPrA. Thus, these two signals are depicted as a function of TPrA concentration (see Figures 6a and 6b). The ECL intensity is proportional up to 10 mmol L^{-1} of TPrA and then levels off (see Figure 6a), giving an R-squared value of 0.993 in the range between 0.2 mmol L^{-1} and 10 mmol L^{-1} of TPrA. This is in good agreement with the earlier results reported.[52, 55] Similarly, the SPR peak wavelength (λ_{min}) is linear up to 10 mmol L^{-1} of TPrA (see Figure 6b), giving an R-squared value of 0.992 in a broader TPrA concentration range between 0.02 mmol L^{-1} and 10 mmol L^{-1}. Clearly, both SPR and ECL responses reach saturation at 20 mmol L^{-1} of TPrA, and the cross-validated ECL and SPR signals featured the reliability of the new sensor. The narrower linear concentration range observed for ECL can be interpreted in two ways. The ECL emission with a peak appearing at 614 nm (see Figure 3) may induce surface plasmon resonance in the nanohole patterned probe,[46] which lowers the ECL peak intensity observed. Alternatively, a smaller flux of TPrA+ radicals is generated at relatively lower TPrA concentrations, and partially quenched by a trace amount of dissolved oxygen molecules.[55]

However, these facts do not impact on the SPR responses, namely the λ_{min} values that are found at 0.0 V vs AgCl/Ag in this system. The SPR signals exhibit a wider linear response than that of (1.8 – 50.0 μmol L^{-1}) on indium tin oxide (ITO) electrodes modified with vertically aligned silica mesochannels[56] and that of (up to 10 μmol L^{-1}) on TiO_2 electrodes modified with $Ru(bpy)_3^{2+}$/CuO nanoparticles.[57] Furthermore, the ESPR peak shift (λ_{max} - λ_{min}) is depicted over the concentration of TPrA (see Figure 6c). The linear detection range is surprisingly extended up to 20 mmol L^{-1} with an R-squared value of 0.993 in the range between 0.02 mmol L^{-1} and 20 mmol L^{-1} of TPrA, offering a new means for the detection of TPrA. These results clearly demonstrate that the novel flow injection ESPR device is a reliable platform for multimodal detection of TPrA in the complicated ECL system. More importantly, this platform can be easily extended to general non-ECL systems for detection of biologically relevant species and explosives, where the concentration could be cross-validated by electrochemical, SPR and ESPR responses.

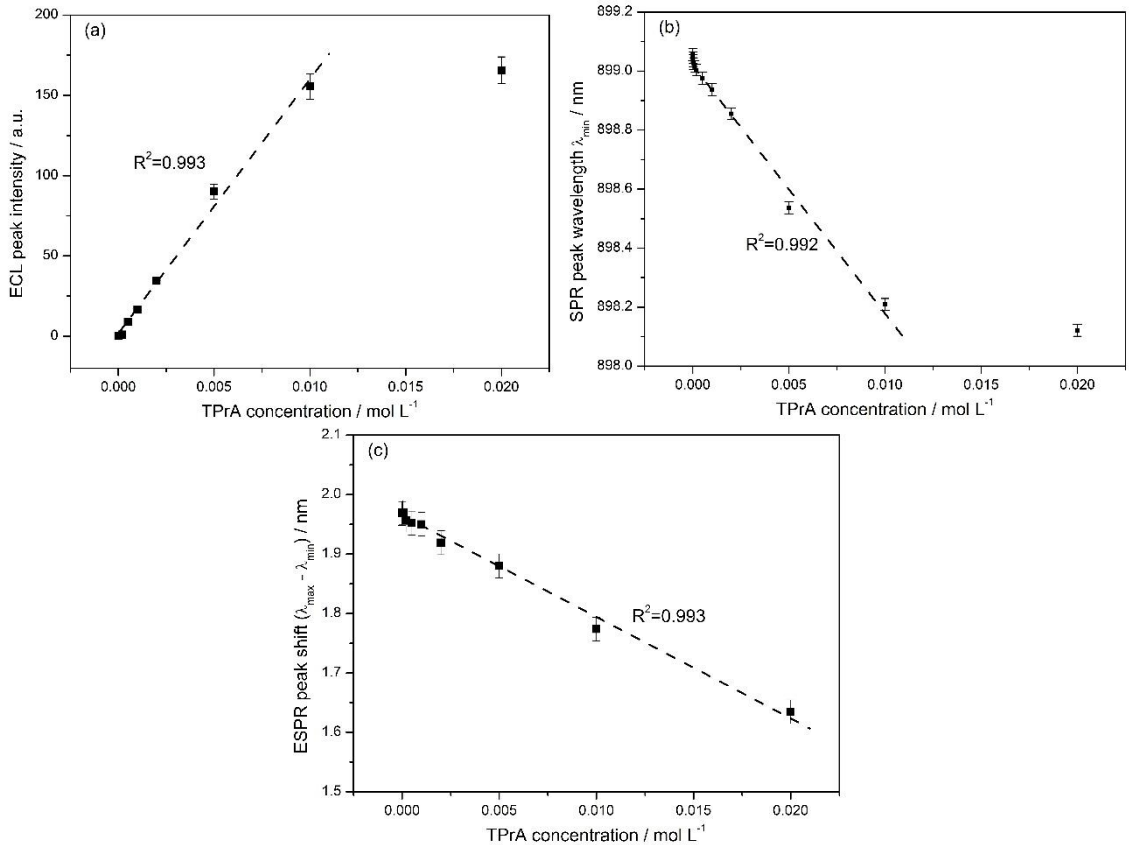

Figure 6. Dependence of (a) ECL peak intensity found above 1.0 V, (b) SPR peak wavelength (λ_{min}) at 0 V, and (c) ESPR peak shift (λ_{max} - λ_{min}) on the concentration of TPrA. Three measurements were conducted at each concentration.

4. Conclusion

We present a versatile flow injection ESPR device by the integration of a plasmonic and conductive fiber optic probe into a PDMS flow channel, where the probe also acts as the working electrode. The optical response through the probe is collected in a transmission mode at normal incidence by the other face-to-face configured fiber to simplify optical system design. The coreactant-based $Ru(bpy)_3^{2+}$ / TPrA ECL system was chosen as a model to first verify electrochemical and ECL performance of the flow injection device. The electrochemically-induced real-time changes in local SPR visualizes the interfacial processes with multi-dimensional information, and provides real-time evidence to support the proposed oxidative-reduction pathway. Furthermore, the ESPR peak shift (λ_{max} - λ_{min}) presents a potentially better means for the detection of TPrA, which greatly extends the linear detection range up to 20 mmol L^{-1} in comparison to 10 mmol L^{-1} achieved by the ECL and SPR methods. Importantly, this device can be easily extended to other non-ECL analytical systems for multimodal and cross-validated detection by electrochemical, SPR and ESPR responses. The novel flow injection ESPR device opens up exciting opportunities to advance fundamental understanding of complicated chemical processes and provide better sensing capabilities, while also offering great advantages such as simplicity, low cost and remote access.

Acknowledgements

The authors acknowledge the financial support provided by the ARC Centre of Excellence for Nanoscale BioPhotonics (CE140100003), ARC Discovery Projects (DP170104367, DP180101581) and the IPAS Pilot Project Funding Scheme (2017). This work was conducted

in part at the Optofab node and South Australian node of the Australian National Fabrication Facility (ANFF).

References

[1] P. Singh, SPR Biosensors: Historical Perspectives and Current Challenges, Sensors and Actuators B-Chemical, 229(2016) 110-30.
[2] S.P. Wang, X.P. Huang, X.N. Shan, K.J. Foley, N.J. Tao, Electrochemical Surface Plasmon Resonance: Basic Formalism and Experimental Validation, Analytical Chemistry, 82(2010) 935-41.
[3] A. Chieng, M. Chiang, K. Triloges, M. Chang, Y.X. Wang, Recent progress in the studies of electrochemical interfaces by surface plasmon resonance spectroscopy and microscopy, Current Opinion in Electrochemistry, 13(2019) 94-9.
[4] A.B. Dahlin, B. Dielacher, P. Rajendran, K. Sugihara, T. Sannomiya, M. Zenobi-Wong, et al., Electrochemical plasmonic sensors, Analytical and Bioanalytical Chemistry, 402(2012) 1773-84.
[5] Y.M. Fang, H. Wang, H. Yu, X.W. Liu, W. Wang, H.Y. Chen, et al., Plasmonic Imaging of Electrochemical Reactions of Single Nanoparticles, Accounts of Chemical Research, 49(2016) 2614-24.
[6] Y. Montelongo, D. Sikdar, Y. Ma, A.J.S. McIntosh, L. Velleman, A.R. Kucernak, et al., Electrotunable nanoplasmonic liquid mirror, Nature Materials, 16(2017) 1127-+.
[7] X.R. Cheng, G.Q. Wallace, F. Lagugne-Labarthet, K. Kerman, Au Nanostructured Surfaces for Electrochemical and Localized Surface Plasmon Resonance-Based Monitoring of alpha-Synuclein-Small Molecule Interactions, Acs Applied Materials & Interfaces, 7(2015) 4081-8.
[8] A. Blidar, B. Feier, M. Tertis, R. Galatus, C. Cristea, Electrochemical surface plasmon resonance (EC-SPR) aptasensor for ampicillin detection, Analytical and Bioanalytical Chemistry, 411(2019) 1053-65.
[9] J. Golden, M.D. Yates, M. Halsted, L. Tender, Application of electrochemical surface plasmon resonance (ESPR) to the study of electroactive microbial biofilms, Phys Chem Chem Phys, 20(2018) 25648-56.
[10] L. Zhou, M.A. Arugula, B.A. Chin, A.L. Simonian, Simultaneous Surface Plasmon Resonance/Fluorescence Spectroelectrochemical in Situ Monitoring of Dynamic Changes on Functional Interfaces: A Study of the Electrochemical Proximity Assay Model System, Acs Applied Materials & Interfaces, 10(2018) 41763-72.
[11] Y. Feng, E.R. Dionne, V. Toader, G. Beaudoin, A. Badia, Odd-Even Effects in Electroactive Self-Assembled Monolayers Investigated by Electrochemical Surface Plasmon Resonance and Impedance Spectroscopy, Journal of Physical Chemistry C, 121(2017) 24626-40.
[12] D.Q. Chen, W.H. Hu, In Situ Investigation of Electrochemically Mediated Surface-Initiated Atom Transfer Radical Polymerization by Electrochemical Surface Plasmon Resonance, Analytical Chemistry, 89(2017) 4355-8.
[13] A.H. Qatamin, J.H. Ghithan, M. Moreno, B.M. Nunn, K.B. Jones, F.P. Zamborini, et al., Detection of influenza virus by electrochemical surface plasmon resonance under potential modulation, Applied Optics, 58(2019) 2839-44.
[14] B.D. Gupta, R. Kant, INVITED Recent advances in surface plasmon resonance based fiber optic chemical and biosensors utilizing bulk and nanostructures, Optics and Laser Technology, 101(2018) 144-61.

[15] A.K. Sharma, A.K. Pandey, B. Kaur, A Review of advancements (2007-2017) in plasmonics-based optical fiber sensors, Optical Fiber Technology, 43(2018) 20-34.
[16] G. Kostovski, P.R. Stoddart, A. Mitchell, The Optical Fiber Tip: An Inherently Light-Coupled Microscopic Platform for Micro- and Nanotechnologies, Advanced Materials, 26(2014) 3798-820.
[17] M. Consales, A. Ricciardi, A. Crescitelli, E. Esposito, A. Cutolo, A. Cusano, Lab-on-Fiber Technology: Toward Multifunctional Optical Nanoprobes, Acs Nano, 6(2012) 3163-70.
[18] Y. Huang, W.Y. Xie, D.Y. Tang, C.L. Du, Theoretical analysis of voltage-dependent fiber optic surface plasmon resonance sensor, Optics Communications, 308(2013) 109-14.
[19] Y.F. Sun, H.Y. Cao, Y.Q. Yuan, Y. Huang, H.L. Cui, W. Yun, Electrically Tunable Fiber Optic Sensor Based on Surface Plasmon Resonance, Plasmonics, 11(2016) 1437-44.
[20] Y. Yuan, T. Guo, X.H. Qiu, J.H. Tang, Y.Y. Huang, L. Zhuang, et al., Electrochemical Surface Plasmon Resonance Fiber-Optic Sensor: In Situ Detection of Electroactive Biofilms, Analytical Chemistry, 88(2016) 7609-16.
[21] P. Niedzialkowski, W. Bialobrzeska, D. Burnat, P. Sezemsky, V. Stranak, H. Wulff, et al., Electrochemical performance of indium-tin-oxide-coated lossy-mode resonance optical fiber sensor, Sensors and Actuators B-Chemical, 301(2019).
[22] J. Dintinger, S. Klein, T.W. Ebbesen, Molecule-surface plasmon interactions in hole arrays: Enhanced absorption, refractive index changes, and all-optical switching, Advanced Materials, 18(2006) 1267-70.
[23] P. Jia, K. Zuber, Q. Guo, B.C. Gibson, J. Yang, H. Ebendorff-Heidepriem, Large-area freestanding gold nanomembranes with nanoholes, Materials Horizons, (2019) DOI: 10.1039/c8mh01302k.
[24] P.P. Jia, H. Jiang, J. Sabarinathan, J. Yang, Plasmonic nanohole array sensors fabricated by template transfer with improved optical performance, Nanotechnology, 24(2013).
[25] A.P. Blanchard-Dionne, M. Meunier, Sensing with periodic nanohole arrays, Advances in Optics and Photonics, 9(2017) 891-940.
[26] N. Polley, S. Basak, R. Hass, C. Pacholski, Fiber optic plasmonic sensors: Providing sensitive biosensor platforms with minimal lab equipment, Biosensors & Bioelectronics, 132(2019) 368-74.
[27] E.M. Zhao, P.P. Jia, H. Ebendorff-Heidepriem, H.Y. Li, P. Huang, D.Y. Liu, et al., Localized surface plasmon resonance sensing structure based on gold nanohole array on beveled fiber edge, Nanotechnology, 28(2017).
[28] P.P. Jia, J. Yang, A plasmonic optical fiber patterned by template transfer as a high-performance flexible nanoprobe for real-time biosensing, Nanoscale, 6(2014) 8836-43.
[29] A.P. Blanchard-Dionne, M. Meunier, Multiperiodic nanohole array for high precision sensing, Nanophotonics, 8(2019) 325-9.
[30] S. Patskovsky, A.M. Dallaire, A.P. Blanchard-Dionne, A. Vallee-Belisle, M. Meunier, Electrochemical structure-switching sensing using nanoplasmonic devices, Annalen Der Physik, 527(2015) 806-13.
[31] J. Lazar, R.R. Rosencrantz, L. Elling, U. Schnakenbereg, Simultaneous Electrochemical Impedance Spectroscopy and Localized Surface Plasmon Resonance in a Microfluidic Chip: New Insights into the Spatial Origin of the Signal, Analytical Chemistry, 88(2016) 9590-6.
[32] K. Nakamoto, R. Kurita, O. Niwa, Electrochemical Surface Plasmon Resonance Measurement Based on Gold Nanohole Array Fabricated by Nanoimprinting Technique, Analytical Chemistry, 84(2012) 3187-91.
[33] S. Li, J.L. Liu, Y.L. Lu, L. Zhu, C.D. Li, L.J. Hu, et al., Mutual promotion of electrochemical-localized surface plasmon resonance on nanochip for sensitive sialic acid detection, Biosensors & Bioelectronics, 117(2018) 32-9.

[34] N.T. Li, Y.L. Lu, S. Li, Q. Zhang, J.J. Wu, J. Jiang, et al., Monitoring the electrochemical responses of neurotransmitters through localized surface plasmon resonance using nanohole array, Biosensors & Bioelectronics, 93(2017) 241-9.
[35] Z.Y. Liu, W.J. Qi, G.B. Xu, Recent advances in electrochemiluminescence, Chemical Society Reviews, 44(2015) 3117-42.
[36] S.E.K. Kirschbaum, A.J. Baeumner, A review of electrochemiluminescence (ECL) in and for microfluidic analytical devices, Analytical and Bioanalytical Chemistry, 407(2015) 3911-26.
[37] G. Valenti, A. Fiorani, H.D. Li, N. Sojic, F. Paolucci, Essential Role of Electrode Materials in Electrochemiluminescence Applications, Chemelectrochem, 3(2016) 1990-7.
[38] M. Sentic, M. Milutinovic, F. Kanoufi, D. Manojlovic, S. Arbault, N. Sojic, Mapping electrogenerated chemiluminescence reactivity in space: mechanistic insight into model systems used in immunoassays, Chemical Science, 5(2014) 2568-72.
[39] M.P. Dinel, S. Tartaggia, G.Q. Wallace, D. Boudreau, J.F. Masson, F. Polo, The Fundamentals of Real-Time Surface Plasmon Resonance/Electrogenerated Chemiluminescence, Angewandte Chemie-International Edition.
[40] K. Imai, G. Valenti, E. Villani, S. Rapino, E. Rampazzo, M. Marcaccio, et al., Numerical Simulation of Doped Silica Nanoparticle Electrochemiluminescence, Journal of Physical Chemistry C, 119(2015) 26111-8.
[41] A.S. Danis, K.P. Potts, S.C. Perry, J. Mauzeroll, Combined Spectroelectrochemical and Simulated Insights into the Electrogenerated Chemiluminescence Coreactant Mechanism, Analytical Chemistry, 90(2018) 7377-82.
[42] T. Xu, H.F. Shi, Y.K. Wu, A.F. Kaplan, J.G. Ok, L.J. Guo, Structural Colors: From Plasmonic to Carbon Nanostructures, Small, 7(2011) 3128-36.
[43] P.P. Jia, J. Yang, Integration of large-area metallic nanohole arrays with multimode optical fibers for surface plasmon resonance sensing, Applied Physics Letters, 102(2013).
[44] W. Gao, X.H. Xia, J.J. Xu, H.Y. Chen, Three-dimensionally ordered macroporous gold structure as an efficient matrix for solid-state electrochemiluminescence of Ru(bpy)(3)(2+)/TPA system with high sensitivity, Journal of Physical Chemistry C, 111(2007) 12213-9.
[45] Y.B. Zu, A.J. Bard, Electrogenerated chemiluminescence. 66. The role of direct coreactant oxidation in the ruthenium tris(2,2 ')bipyridyl/tripropylamine system and the effect of halide ions on the emission intensity, Analytical Chemistry, 72(2000) 3223-32.
[46] J.S. Yuk, E. O'Reilly, R.J. Forster, B.D. MacCraith, C. McDonagh, Demonstration of surface plasmon-coupled emission using solid-state electrochemiluminescence, Chemical Physics Letters, 513(2011) 112-7.
[47] E. Kerr, E.H. Doeven, G.J. Barbante, C.F. Hogan, D.J. Bower, P.S. Donnelly, et al., Annihilation electrogenerated chemiluminescence of mixed metal chelates in solution: modulating emission colour by manipulating the energetics, Chemical Science, 6(2015) 472-9.
[48] M.M. Richter, Electrochemiluminescence (ECL), Chemical Reviews, 104(2004) 3003-36.
[49] R.J. Forster, P. Bertoncello, T.E. Keyes, Electrogenerated Chemiluminescence, Annual Review of Analytical Chemistry2009, pp. 359-85.
[50] J. Zhang, Z. Gryczynski, J.R. Lakowicz, First observation of surface plasmon-coupled electrochemiluminescence, Chemical Physics Letters, 393(2004) 483-7.
[51] M. Janczuk-Richter, M. Piestrzynska, D. Burnat, P. Sezemsky, V. Stranak, W.J. Bock, et al., Optical investigations of electrochemical processes using a long-period fiber grating functionalized by indium tin oxide, Sensors and Actuators B-Chemical, 279(2019) 223-9.
[52] W.J. Miao, Electrogenerated chemiluminescence and its biorelated applications, Chemical Reviews, 108(2008) 2506-53.
[53] W.J. Miao, J.P. Choi, A.J. Bard, Electrogenerated chemiluminescence 69: The tris(2,2 '-bipyridine)ruthenium(II), (Ru(bpy)(3)(2+))/tri-n-propylamine (TPrA) system revisited - A

new route involving TPrA(center dot+) cation radicals, Journal of the American Chemical Society, 124(2002) 14478-85.
[54] A.J. Bard, L.R. Faulkner, Electrochemical Methods: Fundamentals and Applications, 2nd Edition: Wiley, New York; 2000.
[55] H.Z. Zheng, Y.B. Zu, Emission of tris(2,2 '-bipyridine)ruthenium(II) by coreactant electrogenerated chemiluminescence: From O-2-insensitive to highly O-2-sensitive, Journal of Physical Chemistry B, 109(2005) 12049-53.
[56] Z.Y. Zhou, W.L. Guo, L.R. Xu, Q. Yang, B. Su, Two orders-of-magnitude enhancement in the electrochemiluminescence of Ru(bpy)(3)(2+) by vertically ordered silica mesochannels, Analytica Chimica Acta, 886(2015) 48-55.
[57] Z.X. Yan, Z.H. Xu, J.G. Yu, G. Liu, Enhanced Electrochemiluminescence Performance of Ru(bpy)(3)(2+)/CuO/TiO2 Nanotube Array Sensor for Detection of Amines, Electroanalysis, 26(2014) 2017-22.

Artwork

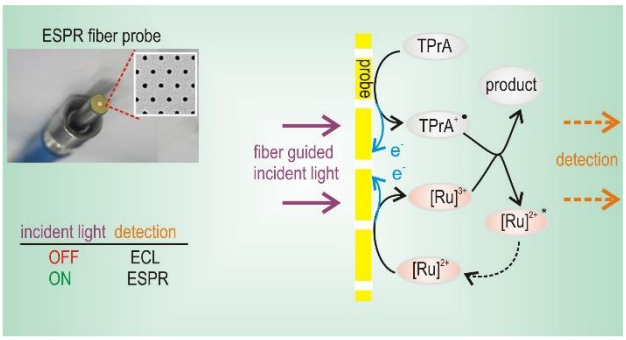
ESPR fiber probe
incident light detection
OFF ECL
ON ESPR
fiber guided
incident light
probe
TPrA
TPrA·+
e-
e-
[Ru]3+
[Ru]2+*
[Ru]2+
product
detection

***Author Biographies**

Jingxian Yu received his PhD in nanoscience and nanotechnology from Flinders University, Australia. He worked as a Roger Pysden Research Fellow at the University of Cambridge, and later at the University of Nottingham, UK as a postdoctoral research fellow. He returned to Australia in 2009 to take up an ARC Australian Postdoctoral Fellowship at the University of Adelaide, where he is currently a Senior Research Fellow & Senior Lecturer at the ARC Centre of Excellence for Nanoscale BioPhotonics (CNBP). His research interests focus on nanomaterials for biological sensing applications, and bio-inspired molecular electronics.

Peipei Jia obtained his PhD in Biomedical Engineering from University of Western Ontario (Western University) in 2014. After a three-year Research Associate at University of Adelaide, he is now working in Topmembranes Technology Co., Ltd., China. His research interests include plasmonic sensing, nanofabrication and membrane technique.

Shengping Wang is currently Professor of Chemistry at China University of Geosciences, following an eight year appointment in research & product development in the lithium battery industry. He is now devoting himself to electrochemical energy storage of materials, electrocatalysis and corrosion.

Heike Ebendorff-Heidepriem received the Ph.D. degree from the University of Jena, Germany, in 1994. She received the Weyl International Glass Science Award and the prestigious Marie Curie Individual Fellowship in 2001. During 2001-2004 she was with the Optoelectronics Research Centre at the University of Southampton, UK. Since 2005, she has been with the University of Adelaide, Australia. Currently, she is the Deputy Director of the Institute for Photonics and Advanced Sensing (IPAS). She is also Senior Investigator of the ARC Centre of Excellence for Nanoscale BioPhotonics (CNBP). Her research focuses on the development of novel optical glasses, specialty optical fibres, surface functionalization and sensing approaches.

Andrew Abell graduated from the University of Adelaide with BSc(Hon) and PhD and then undertook a postdoctoral fellowship at the University of Cambridge. He held a professorship at the University of Canterbury before returning to the University of Adelaide in 2007, where he is currently Professor of Chemistry and node director of the ARC Centre of Excellence for Nanoscale Biophotonics (CNBP). He is past Head of School of Chemistry and Physics at the University of Adelaide and recipient of Royal Australian Chemical Institute Adrien Albert Prize and the Alexander R. Matzuk Prize and Lecture in Drug Discovery (Baylor College of Medicine, Houston).

Electrochemical Plasmonic Optical Fiber Probe for Real-time Insight into Coreactant Electrochemiluminescence

Jingxian Yu',[a,*] Peipei Jia, [a] Shengping Wang, [b] Heike Ebendorff-Heidepriem, [a] and Andrew D. Abell [a]

[a] ARC Centre of Excellence for Nanoscale BioPhotonics (CNBP), Institute of Photonics and Advanced Sensing (IPAS), School of Physical Sciences, The University of Adelaide, SA 5005, Australia

[b] Faculty of Materials Science and Chemistry, China University of Geosciences, Wuhan 430074, China

Conflict of Interest

The authors declare no conflict of interest.

Declarations of interest:

None

*Credit Author Statement

AUTHOR CONTRIBUTIONS

Jingxian Yu performed conceptualization and writing – original draft preparation;

Peipei Jia: conceptualization, methodology;

Shengping Wang: methodology;

Heike Ebendorff-Heidepriem and Andrew D. Abell performed writing – review and editing.

Highlights

- A nanohole array patterned gold film allows for collection of plasmonic responses in transmission mode
- A plasmonic while conductive fiber tip enables electrochemical manipulation of SPR excitations
- Multimodal signals (CV, SPR and ECL) generated on the optical fiber tip
- Real-time interfacial information for ECL was unravelled by correlation of multi-dimensional signals
- The fiber optic ESPR device presents real advantages over convential prism-based ESPR approach